Release and fragmentation of aggregates to produce heterogeneous, lumpy coma streams

B. C. Clark,[1] S. F. Green,[2] T. E. Economou,[3] S. A. Sandford,[4] M. E. Zolensky,[5] N. McBride,[2] and D. E. Brownlee[6]

Received 9 July 2004; revised 1 October 2004; accepted 9 November 2004; published 24 December 2004.

[1] The unpredicted heterogeneity in particle number density in the coma of Wild 2 is consistent with delayed fragmentation to produce small particles from larger aggregates initially ejected from the cometary nucleus. The resultant heterogeneous inner coma results in stochastic variations in particle number and size distribution. Fragmentation can be accelerated after aggregate release by enhanced heating and one or more additional factors such as abrupt depressurization, phase transitions, exothermic chemical reactions, centrifugal forces, and electrostatic repulsion. Certain predicted characteristics of such in-flight disaggregation in coma particle streams correspond to known cometary phenomena. *INDEX TERMS:* 6015 Planetology: Comets and Small Bodies: Dust; 6210 Planetology: Solar System Objects: Comets; 6215 Planetology: Solar System Objects: Extraterrestrial materials; 6094 Planetology: Comets and Small Bodies: Instruments and techniques; 2129 Interplanetary Physics: Interplanetary dust; *KEYWORDS:* cometary dust, Stardust, 81P/Wild 2, Dust Flux, DFMI

Citation: Clark, B. C., S. F. Green, T. E. Economou, S. A. Sandford, M. E. Zolensky, N. McBride, and D. E. Brownlee (2004), Release and fragmentation of aggregates to produce heterogeneous, lumpy coma streams, *J. Geophys. Res.*, *109*, E12S03, doi:10.1029/2004JE002319.

1. Introduction

[2] In his pioneering description of the development of the cloud of dust and gas that surrounds the active cometary nucleus, *Whipple* [1951] proposed and analyzed the "conglomerate" model, whereby more refractory particulates are enmeshed in an icy matrix but released individually as the surface ice sublimates under solar insolation. As observational opportunities have increased, numerous comets have been seen to split or form multiple daughter nuclei, and some to even undergo virtually complete disruption. Such large-scale fragmentation may be symptomatic of processes that can also occur at the smaller scale.

[3] The Stardust mission's transect of the 81P/Wild 2 coma [*Tsou et al.*, 2003, 2004; *Brownlee et al.*, 2004] revealed not only visual images of dozens of small jets [*Brownlee et al.*, 2004; *Sekanina et al.*, 2004], but also discovered strong fluctuations in particle number density in 100 milliseconds or less [*Tuzzolino et al.*, 2004] corresponding to distances considerably less than one km. Regions of high particle density were sometimes interspersed by gaps within which almost no particles were detected. Although many periods of high particle flux in the data may be explicable as transversals of conical sheets created by individual jet streams [*Sekanina et al.*, 2004], the short-duration fluctuations ("bursts") within these streams, bolster a number of separate lines of evidence for a model in which some or many particles are released from the nucleus initially as larger aggregates which then disaggregate along their trajectory as they pass into the outer coma.

[4] Voids in particle number density will occur between clumps if subfragments from each parent aggregate particle are released at velocities low compared to the aggregate's cometocentric velocity. Daughter products from multiple successive fragmentations of the initial aggregate will thus move together, unless they are still within the near-nucleus region in which drag forces from expanding cometary gases are significant and can further accelerate the finer grains. In either case, an inner coma with a nonuniform spatial dust density would result.

2. Previous Models of Jets

[5] Sharp-boundaried zones of high particle concentration have often been interpreted to be the result of geometrically collimated "jets" of particles, presumably caused by particles spewing from a deep crevasse or tunnel.

[6] Alternatively, it has been proposed that apparent bunching of cometary dust grains results from entrainment of dust in preferred directions of gas flow inevitable for a nonspherically shaped nucleus, as predicted from

[1]Lockheed Martin, Denver, Colorado, USA.
[2]Planetary and Space Sciences Research Institute, Open University, Milton Keynes, UK.
[3]Laboratory for Astrophysics and Space Research, Enrico Fermi Institute, University of Chicago, Chicago, Illinois, USA.
[4]NASA Ames Research Center, Moffett Field, California, USA.
[5]NASA Johnson Space Center, Houston, Texas, USA.
[6]Astronomy Department, University of Washington, Seattle, Washington, USA.

0148-0227/04/2004JE002319$09.00

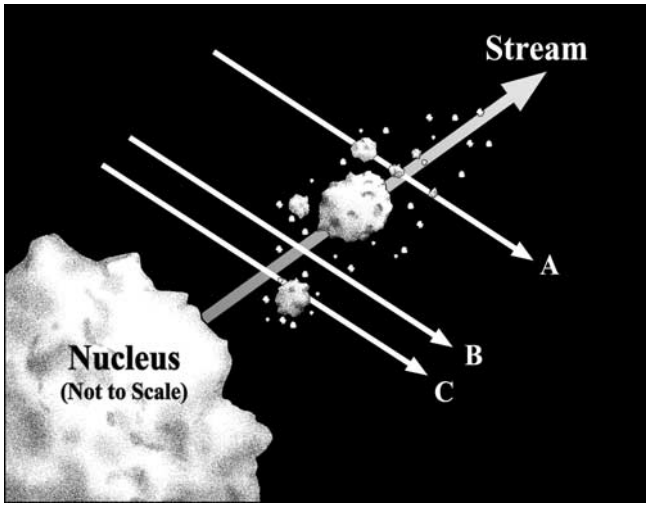

Figure 1. Multiple aggregates are released from the cometary surface to form a stream of progressively increasing numbers of daughter particles, with decreasing average particle size. Sampling by passing through such a stream would give highly variable results: paths A and C will detect narrow streams but at different times and azimuths with respect to the surface origin location, while path B would indicate a void, i.e., few or no particles. Other paths could detect two substreams, as well as zones rich in either large or small particles.

detailed 3-D modeling of the appropriate gas dynamics [*Crifo et al.*, 2002]. The very large number of observed jets will challenge such modeling in view of the highly imperfect knowledge of the detailed shape of the nucleus of 81P/Wild 2.

[7] Another suggested mechanism for the strong collimation effect observed in high-resolution images of the Borrelly inner coma is due to the supersonic nozzle effect for expulsion of particles from subsurface, gas-charged accumulation reservoirs through narrow orifices [*Yelle et al.*, 2004].

[8] However, narrow peaks in particle number density observed in situ need not necessarily imply such strong degrees of collimation. Highly segregated zones could arise instead from a ''clumpy'' stream of coma aggregate particles undergoing progressive fragmentation, as proposed here and schematically portrayed in Figure 1. As seen by the multiplicity of possible outcomes, stochastic variations in sampling occur depending not only on the spatial heterogeneity within the stream but also the timing of the flythrough. In this way, clusters of particles at a fine substructure (the ''bursts'') can occur within a far less-collimated primary jet. Even a jet observed telescopically might be due to a release of a relatively large amount of material in a short period of time and subject to the same directional path by gas entrainment, but spread along its trajectory by different accelerations for different particle sizes. As fragmentation proceeds, the optical signature reflects the motion of the primary source aggregates and appears as if from a collimated source. Longer-term observation of each jet is required to ascertain the contributions of various proposed mechanisms since flyby missions are intrinsically limited to only some minutes of observation time.

3. A Fragmentation Model

[9] Emission from the surface could consist of release of both fine-grained dust from a smoothly sublimating surface and aggregates of dust and ice as individual larger grains. In the latter case, factors other than simple sublimation, as described in section 4 below, would be significant. If it were possible to follow the time-sequence of a single stream of particles, the release of aggregates which subsequently fragmented would produce a variable particle size distribution with respect to position along radial trajectories from the surface to the outer coma.

[10] Once released from the nucleus, aggregates are suddenly in a different environment. Solar heating and electrostatic charging will occur from all directions as they tumble freely in space; topographic shadowing and nighttime occultation by surrounding terrain no longer occur; conduction paths (solid and gas) to the deep, cold nucleus interior are interrupted; the entire clump is exposed to relatively higher vacuum conditions; expanding gas from the adjacent surface accelerates material and collisions may occur.

3.1. Modeling of Clusters

[11] A cluster of particles derived from a single aggregate is modeled to surround its center of mass (c.m.) isotropically out to a spherical radius, r, as shown in Figure 2. Each particle's distance from the c.m. depends on its separation

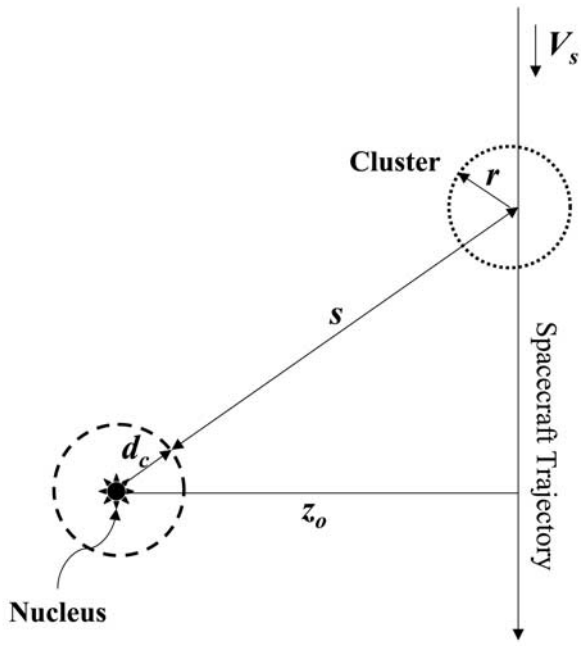

Figure 2. Schematic of cluster, comet nucleus, and spacecraft flyby trajectory. The spherical cluster is shown with the trajectory passing through its center as a simplifying approximation, since r $\ll$ s for the Stardust flyby conditions. In calculations, the path through the cluster is taken as the average chord, equation (4).

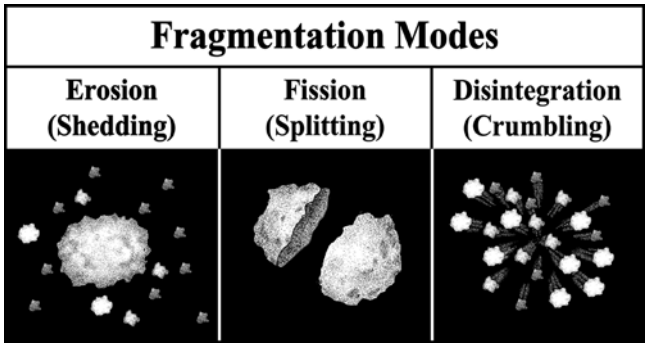

Figure 3. Fragmentation modes are modeled in three phenomenological forms.

velocity, v, and the time since its release. For a cluster moving out to a distance, s, beyond the region where gas coupling ceases to accelerate the particles (d_c, the coupling distance), the maximum radius of expansion (from the earliest particles released), is derived from the time of flight, τ,

$$\tau = \frac{r}{v} = \frac{s}{V_a}, \tag{1}$$

where V_a is the terminal velocity (cometocentric) of the aggregate as it reaches the distance d_c. By trigonometry, the value of s is given by

$$s = \sqrt{z_0^2 + (V_s t)^2} - d_c, \tag{2}$$

where V_s is the spacecraft velocity relative to the nucleus (6.1 km/s for Stardust), t is time from closest approach, and z_0 is the distance from the surface of the nucleus at closest approach (236 km for the Stardust flyby of Wild 2).

[12] The spacecraft's path can intersect the cloud of particles along any chord of the sphere. The path length, L, through a cluster is determined by the time interval, Δt, during which the spacecraft passes through the cloud and particles are detected:

$$L = V_s \Delta t. \tag{3}$$

[13] For a spherical cluster, the path length distribution is triangular, with average path length, $\bar{L}$, of the chord,

$$\bar{L} = \frac{4r}{3}. \tag{4}$$

3.2. Emission of Particles

[14] Fragmentation encompasses at least three likely modes (Figure 3). (1) Shedding or sloughing of individual grains as ices sublimate is a surface process, reminiscent of erosion and deflation on planetary bodies with dynamic atmospheres. (2) A fission or shattering event, in which an aggregate splits into large subaggregates, a process that would be typically asymmetric. (3) Direct disintegration into many small particles can occur via explosive-like chemical or phase-change energy release, electrostatic disruption [*Hill and Mendis*, 1980], centrifugal breakup, or simply as a result of quasi-uniform weakening of the matrix material as it heats up.

[15] Since all three modes, and perhaps others, may be active at any given time, the number of individual particles grows at least geometrically, but probably much faster, as fragmentation proceeds. Fragmentation is generally expected to be self-reinforcing. The breakup of one aggregate into one-thousand smaller aggregates results in ten times the specific heating rate of the material. At the location of the Wild 2 encounter, 1.86 AU from the sun, a 1-mm ice-dust aggregate (mass density = 2 g cm^{-3}; albedo = 4%) would be heated at the rate of 0.2 W g^{-1}, but its 30-μm daughter fragments would together experience a solar thermal input of 7.2 W g^{-1}. Specific reradiation area partially compensates, increasing by the same large factor, but net heating is dependent on the magnitude of this difference and the absorptivity: emissivity ratio of the grains. As aggregates are reduced in size and fall below the infrared wavelengths corresponding to efficient blackbody emission, their temperatures increase even faster because of the inhibition of reradiation [*Hanner and Campins*, 1986].

[16] After an aggregate particle moves outward, it potentially will also be subject to bombardment by smaller particles which were emitted later but have become accelerated to much higher velocities by gas drag. Because the relative velocity at which they are overtaken can be as high as 100's of m/s, the larger particles can suffer further fragmentation or erosion.

3.2.1. Fission Mode

[17] With fission, each aggregate splits into large fragments, and these then subsequently divide to result in more fragments. For binary fission, after 7 generations of splitting there are 128 fragments, all derived from the one parent particle.

$$N_f = 2^g \text{ and } g = \frac{\tau}{\tau_g}, \tag{5}$$

where N_f is the number of fragments as a function of flight time of the center of mass of the cluster, τ, and the average time between generations, τ_g.

[18] Combining with equation (1), the number of fission fragments is

$$N_f = 2^{\wedge}\left(\frac{s}{V_a \tau_g}\right), \tag{6}$$

where ^ denotes exponentiation and the number density, n_f, in the cluster is

$$n_f = \frac{3N_f}{4\pi r^3}.$$

[19] Next, consider the admittedly oversimplified but instructive case of a constant fragmentation ratio, such that for each fission event a larger particle with fraction p of the mass, and a smaller particle with fraction q, are produced. If we follow only the largest particle, by g generations it will have been reduced to a mass relative to the original particle

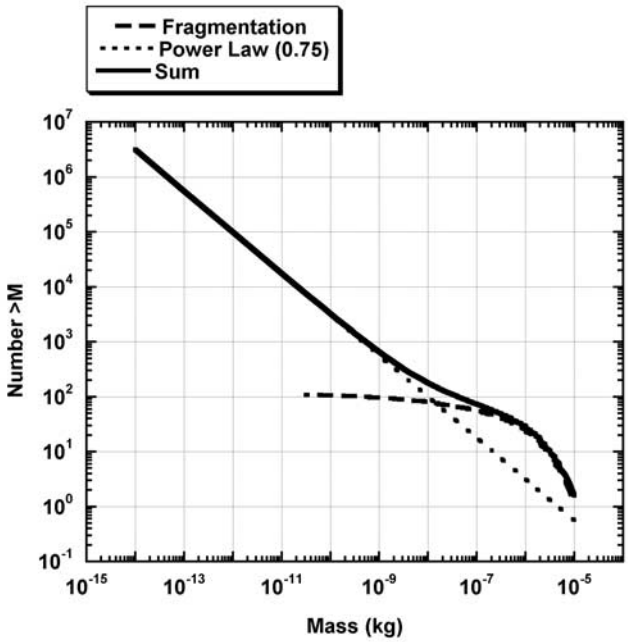

Figure 4. Combined (sum) mass distribution function for power law distribution for small particles and a fragmentation model for large particles. The large particle excess that has been observed for both Halley and Wild 2 as a flattening then final steepening of the distributions is understood as the natural result of a fragmentation pattern.

of p^g. Likewise, the smallest particle will have relative mass q^g. The mass of a particle at the 9th generation, whose predecessors were the larger particle six times and the smaller fragment three times, would be p^6q^3. Generalizing, it can be seen that at generation g the particle population is derivable from the binomial distribution,

$$(p+q)^g, \tag{7}$$

for which the well-known binomial coefficients provide an enumeration of the number of particles of the same size. In reality, the fragmentation ratio is different each time a split occurs, and no two aggregates are expected to be the same. This formulation provides, however, insight into the types of size distributions to be expected for a binary fission model. For example, the cumulative mass distributions from the 1st through the 7th generation (constant fragmentation ratio, $p = 0.8$, $q = 0.2$) for three starting particles (relative masses of 2, 1, 0.5) is plotted in Figure 4. In a steady state situation, where source aggregates continue to be fed into the coma, this example could relate to the integrated results of a flythrough of several clusters at various stages of fragmentation. Combined with a power law mass distribution of $\alpha = 0.75$ for small particles, the log-log plots in Figure 4 of the summed curves have a very similar shape as the data obtained for comets 1P/Halley and 81P/Wild2 [*Green et al.*, 2004, Figure 8], lending credence to the suspicion that the excess at high masses represents aggregates undergoing fragmentation.

[20] Only for the special, unrealistic case of $p = 0.5$ does the fragmentation slope become a straight line in a log-log plot. This case is highly improbable because a 0.5/0.5 fragmentation ratio is the most energetic, requiring a split with the maximum amount of surface area at the separation surface, and also because the number of ways in which a split can be this precise is lower than all the other alternatives.

[21] Increases in the number of particles cannot follow equation (5) indefinitely because ultimately the smallest fragments will be at the irreducible size of the primordial dust grains embedded in the comet. The inflection in mass size distribution curves for comae of both comets Halley and Wild 2 seems to occur at about 10^{-10} kg [*Green et al.*, 2004, Figure 8]. Particle sizes extend down to at least the m_1 threshold of 10^{-14} kg. If the original mass of the primary aggregate released from the nucleus is M_a, then the number of generations for which the smallest particle becomes mass m is derived from

$$q^g = \frac{m}{M_a},$$

which, for a cm-sized M_a of 1 g, and our example of $q = 0.2$, is reached for the two values of m in 16 to 22 generations, respectively. For the largest fragment to be reduced to just the inflection mass requires over 100 generations of binary fission.

[22] As the aggregate moves outward, the effect of fission will progressively increase the surface area of the fragments. Assuming the mass density, ρ, of all individual subfragments are the same, the surface area of the ensemble is proportional to the 2/3 power of mass,

$$A = \sum_i \frac{3\rho}{4} m_i^{2/3}. \tag{8}$$

[23] Detailed branching calculations using equations (5) and (8) show that after 10 generations the resulting 1,024 particles have a total area 4 to 10 times larger than the original surface area (for fragmentation ratios of 0.5/0.5 to 0.9/0.1, per generation). After 10 more generations there will be 10^6 particles, with 16 to 100 times total surface area of the particles in the cluster relative to the original primary aggregate released from the nucleus. With higher total surface area, as noted in the preceding discussions, rates will more quickly reach equilibrium. From the well-known exponential dependence on temperature, sublimation will increase rapidly (accelerated shedding) and total heat absorption may be higher, resulting in shorter time intervals between successive generations.

3.2.2. Erosion Mode (Shedding)

[24] Individual dust grains that are shed from an aggregate particle while still in the relatively gas-rich zone near the surface of the nucleus will be accelerated by gas drag to high speeds relative to that of the aggregate itself. Conventional models assume all gas is released at the cometary surface and therefore overestimate the gas density since by the aggregate release model a significant fraction of the volatiles may be carried away in solid form and released at distances where the inverse-square effect results in a diminished gas density. The effect will be a smaller d_c.

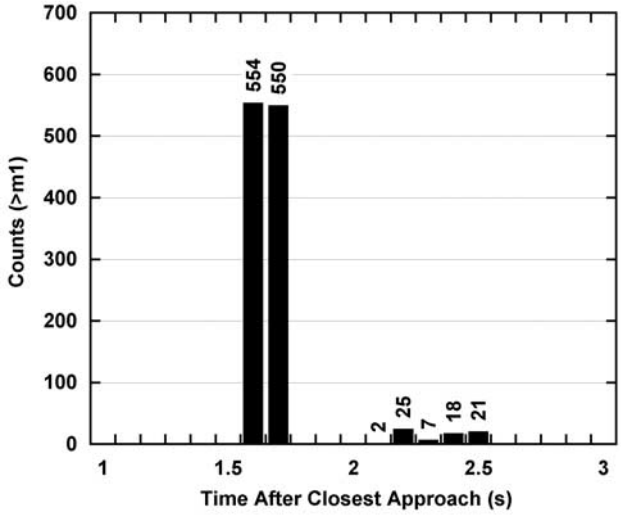

Figure 5. Bursts at closest approach have considerably different properties, including amplitude, width, gaps, and size distributions, even though correlated to a single jet (β jet of *Sekanina et al.* [2004]).

[25] For this mode, the release of dust grains occurs as a surface process, unlike the bulk process of fission fragmentation. As assumed in previous models of comet surface emission, the observed dust size distributions may reflect the conditions of grain formation and evolution. For an empirical approach, we can utilize the steepest portion of the low end of the mass distribution curves from comet measurements, and assume it represents the intrinsic size distribution of nonvolatile grains embedded in the cometary nucleus. The exponent for the Wild 2 late event is 1.13 [*Green et al.*, 2004].

[26] The output of primary grains by solar insolation on the surface of an aggregate will be proportional to the exposed area. The number density due to erosional shedding of grains, n_s, by ablation of the cementing ice is given by

$$n_s = kA(\tau), \tag{9}$$

where $A(\tau)$ is the exposed area of the sum of the particles in the cluster as a function of flight time τ, and k is the proportionality constant to relate the amount of emission per unit area from a specific location on the cometary surface to produce a measured number density at the time of the observation.

3.2.3. Disintegration Mode

[27] The occurrence of bursts of the smallest particles, but with no associated larger particles, would be indicative of the possible importance of this mechanism. Indeed, the late event does have this characteristic [*Tuzzolino et al.*, 2004; *Green et al.*, 2004]. However, as we shall discuss below, this can also be explained as the result of sufficient time for the first two modes to go to completion. Thus no incontrovertible, direct observation of a disintegration mode has been forthcoming to date. Because there is some expectation for this modality based on laboratory experiments (see section 4), it is included in the formulation for completeness, but is not be assigned a value at this time.

3.3. Application of Fragmentation Model to Wild 2

[28] A number of predictions of the fragmentation and cluster model can be compared with the data obtained during the Wild 2 flyby.

3.3.1. Pseudocollimation

[29] Explaining the bursts in DFMI data is extremely difficult using traditional jet concepts because of the extreme collimation that is implied. For a burst of width Δt, the angular spread, ϑ, at the distance detected is given by

$$\vartheta = \frac{2r}{(s + d_c)}.$$

[30] Invoking equations (2), (3) and (4),

$$\vartheta = \frac{3\Delta t}{2\sqrt{\left(\frac{z_o}{V_s}\right)^2 + t^2}}. \tag{10}$$

[31] For the close encounter, the DFMI m_1 channel records 1104 counts in just two 0.1 s recording intervals, at +1.65 s after encounter as seen in Figure 5. From equation (10), the value of ϑ is 7.7 milliradians (mrad). If caused by collimation from a crevasse, the depth:diameter ratio would have to be about 130. Obviously, geometric collimation is an untenable model because solar illumination would be extremely brief for any reasonable rotation rate of the nucleus. Also if, as will be argued in section 3.3.3, the Δt is actually much smaller than 0.2 s for this burst, then the narrowness of the beam is even less than calculated above. All other events detected close-in (within 30 s of closest approach) by the DFMI are bursts of 0.1–0.2 s, with the exception of the event centered at +2.3 s, with width of 0.5 s. For this case, the angular width is 19 mrad (1.1°), and a collimation aspect ratio of 50:1 would still be required. Even the smallest particles detected near closest approach and with DFMI's lowest-mass threshold always occur in bursts, rather than the quasi-continuum expected. With a larger detector area, a minor continuum could be measured at statistical significance, but none is evident in this data set.

[32] The late event, centered at 697 s, has a total width of 91 s. The angular spread, by equation (10) is 0.2 radians (11.7°), requiring a geometric collimation of a more reasonable 5:1. However, this event is actually composed of a large number of subclusters (see section 3.3.4), each of which is quite narrow (the largest being less than 0.8 s wide, or 1.8 milliradian). Thus the total event, and its associated 5:1 geometric collimation, may reflect the activity of a single source.

3.3.2. Mass Sizing of Aggregates for Cluster Genesis

[33] The particle number density, n, is derived from the measured flux using the observed counts, C, in time interval Δt for a detector sensitive area, a, by taking into account the velocity of the instrument (spacecraft), which

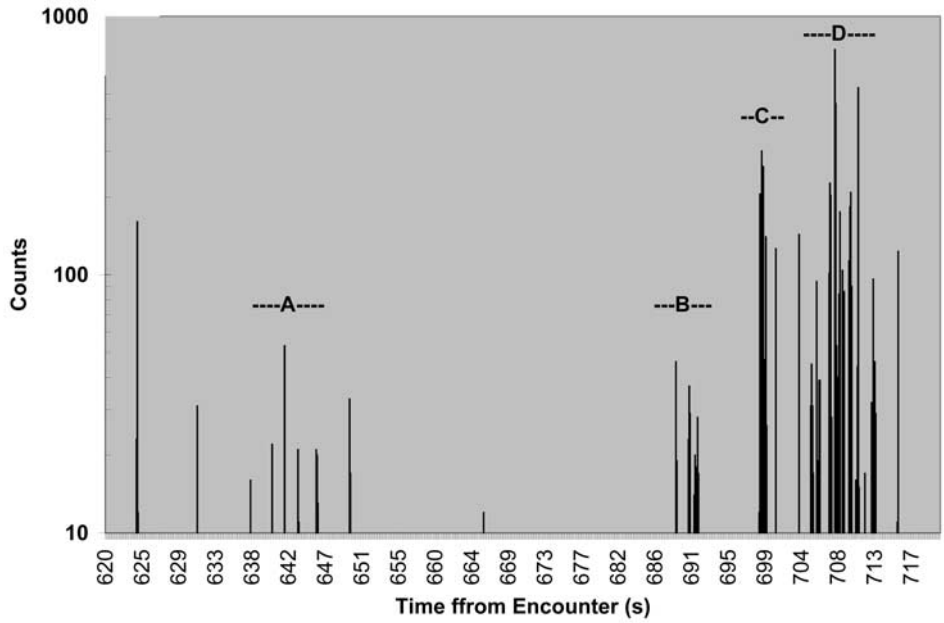

Figure 6. Counts above m1 threshold for Late Event. Some of the 33 clusters identified (see text for criteria) are not evident in this graph because of low amplitude or time clumping. See Table 1 for a complete tabulation.

is sufficiently high that particle cometocentric velocities can be neglected,

$$n = \frac{\phi}{V_s}, \tag{11}$$

where

$$\phi = \frac{C}{a\Delta t}.$$

[34] The inferred minimum mass, M_c, in the cluster is

$$M_c \geq \frac{4}{3}\pi r^3 n m_1, \tag{12}$$

where m_1 is the mass threshold of the highest sensitivity channel (9.8×10^{-15} kg) of the DFMI. For several reasons, this inferred mass is a minimum: (1) data are for mass thresholds, and larger particles may carry most of the mass; (2) the cluster may be larger than the assumed value of a geometrically averaged chord; (3) the model predicts a higher density of particles in the inner regions of the cluster, which may not be sampled by the flythrough.

[35] Combining equations (3), (4), and (11) yields

$$M_c \geq \frac{9}{16}\pi \frac{C m_1 (V_s \Delta t)^2}{a_1}. \tag{13}$$

3.3.3. Near Encounter Jet

[36] Fully 60% of the small particles (m1 threshold) detected during all of the flyby except for the late event were detected in two adjacent 0.1 s time intervals, as seen in the logarithmic plot of Figure 5. This burst possibly could be due to a disintegration mode event since no acoustic-channel detections occurred during this time increment, even though AC counts were recorded both immediately prior and subsequent to it. Both it and the second small cluster near it, occurring at 2.3 s, correspond to the β jet of *Sekanina et al.* [2004], yet they are clearly separate bursts because there are three time intervals with no detected particles that separate them. Indeed, the second cluster is broader even though a factor of 15 less intense. Their proximity to one another, in relative isolation from other events around closest approach [*Tuzzolino et al.*, 2004], implies that they could represent two subclusters of a cluster begun by a single aggregate released from the comet.

3.3.4. Late Event

[37] For analysis of the late event occurring after +620 s, Figure 6, criteria were set to identify clusters. At least 10 counts had to be observed in one or adjacent measurements. Many intervals with lower counts were also observed, but not taken as a cluster. When there was a question whether a decrease in counts demarked a boundary between two clusters, a conservative 3-sigma criterion was imposed to avoid false positives solely due to statistical variation. At least 33 clusters were identified in this late event; only 5 of these had less than 33 counts, and 3 more cases would have passed a 2-sigma test but not the 3-sigma test. In addition, many cases were identified where high counts were immediately flanked by very low counts. Because of expected inverse-square variations, the only way this is possible for this model is if they were actually bunched tighter than the 610 m resolution limit of the system. This is indirect indication that individual clusters may have even finer substructure that could not be probed by the 0.1 second minimum timing interval. Thus 33 is a strong lower limit for

Table 1. Cluster Analysis for Late Event

Cluster	t, s	C, counts	S, km	M_c, g	Δt, s	r, km
1	623.9	195	3806	2.51	0.20	0.9
2	631.1	43	3850	1.25	0.30	1.8
3	634.9	12	3873	0.35	0.30	1.8
4	637.5	17	3889	0.08	0.12	0.7
5	640.1	33	3905	0.24	0.15	0.9
6	641.6	57	3914	0.18	0.10	0.6
7	643.2	33	3924	0.43	0.20	1.2
8	645.5	54	3938	1.57	0.30	1.8
9	649.4	50	3961	0.52	0.18	1.1
10	665.5	12	4060	0.04	0.10	0.6
11	678.4	18	4138	0.17	0.17	1.0
12	688.6	84	4200	6.77	0.50	3.1
13	689.7	13	4207	0.38	0.30	1.8
14	690.2	108	4210	8.70	0.50	3.1
15	691.0	118	4215	19.71	0.72	4.4
16	698.8	644	4263	33.20	0.40	2.4
17	699.1	274	4265	1.07	0.11	0.7
18	699.4	234	4266	12.06	0.40	2.4
19	700.6	128	4274	0.41	0.10	0.6
20	703.4	144	4291	0.46	0.10	0.6
21	704.9	130	4300	8.48	0.45	2.7
22	705.5	117	4304	1.51	0.20	1.2
23	705.9	91	4306	2.64	0.30	1.8
24	707.1	565	4313	22.30	0.35	2.1
25	707.8	1274	4318	50.28	0.35	2.1
26	708.3	317	4321	10.46	0.32	2.0
27	708.6	286	4322	14.74	0.40	2.4
28	709.6	597	4329	30.78	0.40	2.4
29	710.5	625	4334	50.34	0.50	3.1
30	711.3	30	4339	2.42	0.50	3.1
31	712.1	34	4344	0.44	0.20	1.2
32	712.3	199	4345	12.98	0.45	2.7
33	715.3	134	4363	0.73	0.13	0.8

the number of clusters observed for the late event. Applying equation (13) to each of the 33 clusters, Table 1 shows that the smallest mass for a given cluster is found to be 40 mg, while two clusters are slightly in excess of 50 g, and two more are at 30 g. Applying the same equation to the entire event yields a M_c of 18 tonnes, i.e., the disaggregation products of an object formerly 3.3 m in diameter if its bulk density was 1000 kg/m^3. However, for an implied super-cluster of diameter 900 km, the volume that is sampled by the m_1 PVDF detector is trivially small, and the measured counting profile would surely be different for alternative intersection paths through the super-cluster. It is also not possible, of course, to ascertain if the primary object was fully disaggregated at the time of the flyby, or a larger parent object remained in the vicinity.

[38] Hierarchy of cluster formation seems to be evidenced at several places in the data. For example, the data naturally form four groups, as indicated in Figure 6. These are interpreted as indications of earlier fragmentation, while the 33 individual clusters represent subsequent fragmentation patterns. In principle, a sequence of events could be traced back generation-by-generation, with the possibility of estimating sizes and lifetimes of various subaggregates. For example, groups C and D may be derived from a relatively recent split that occurred in the ratio of 1:4 in mass. However, there is an important limitation due to the nature of flythrough observations: only clusters along the velocity vector are sampled. Contributory clusters could be nearby, but offset in the cross-track directions by a distance small compared to cluster sizes (610 m for this resolution) but large compared to feasible sensor sizes for a finite spacecraft size (<1 m in circumscribed diameter). We interpret these data as clear evidence of such hierarchy, even though it cannot be fully specified.

3.3.5. Cluster Sizes and Cometocentric Distance

[39] According to this model, clusters should increase in width as the particle cloud recedes from the comet nucleus, in accordance with the ratio of the separation velocity, v, and motion of the center of mass of the cluster itself, V_a. From equations (1), (3) and (4),

$$\frac{v}{V_a} = \frac{3V_s\Delta t}{4s},$$

where s is given by equation (2).

[40] Clusters at the close encounter distance are typically restricted to a single timing interval of 0.1 s, corresponding to a (v/V_a) ratio of 0.003. However, the cluster at 2.3 s is about 5 times this width, for a ratio as high as 0.013. The late event is much broader, but group A (clusters 4 to 8, Table 1) in Figure 6, may have been an early released fragment of the larger parent aggregate, and gives a v/V_a ratio of 0.008. Hence these clusters are of the same general order in terms of spreading rate, and the separation velocities are accordingly constrained. Narrower, intense clusters in this event indicate late-released aggregates that have had less time to disperse their daughter particles.

3.4. Predictions of the Fragmentation Model

[41] This model predicts many semi-quantitative aspects of coma structure that were actually observed by the Stardust flyby of Wild 2. The ratio of large particles to small particles should be higher near the nucleus, which is exactly as observed since there are almost exclusively m1 counts in the late event cluster at ~4000 km. The coma can be stochastically heterogeneous, even for a given jet, which is seen clearly for the β jet. When many large fragments are produced, they can produce subsequent clumpiness in the fine particles shed from them as they move apart. This is clearly observed in the late event. Finally, the clumpiness should provide an apparent collimation or co-registering of particles that may not be consistent with the mechanism(s) of jet formation.

4. Aggregate Release

[42] We take these data as the strongest evidence for particle fragmentation at Comet Wild 2, a view that has now been embraced by *Tuzzolino et al.* [2004], *Sekanina et al.* [2004], *Green et al.* [2004], and *Levasseur-Regourd* [2004]. In addition, there are many other lines of evidence relevant to release of aggregate particles from the surface of a comet nucleus.

[43] Initial release of an aggregate could be due to thermal stress, internal gas pressure, turbulence in a confined cavity, or other factors. Prior thermal cycling of the surface of the comet nucleus may lead to creation of peds (natural clods). As is well known in the soil sciences, a variety of processes commonly result in soil structure characterized by peds whose scale far exceeds the grain size distribution of the constituent soil particles themselves.

Pummeling by large and small impactors will produce fracture networks in the cold, brittle surface region. In addition, mass wasting can result in accumulations of prefragmented comet talus debris [*Britt et al.*, 2004].

[44] Solar heating of a cometary nucleus can induce not only surface sublimation but also mobilization of subsurface volatiles to build internal forces leading to mechanical disruption of a low-porosity matrix. Experience with placing powdered material in vacuum chambers has led to careful prepreparation protocols in many laboratories to prevent explosive venting due to delayed devolatilization [*Baird et al.*, 1977]. Such experiences, though common, are seldom reported. Hartmann has documented similar phenomenology of gradual buildup and recharge of gas pressure in granular regolith-simulating layers to result in episodic violent disruption even from basaltic powders of very low-volatile content (trapped air and adsorbed H_2O), and proposed an analogy for cometary surface eruption and particle release [*Hartmann*, 1993]. Experimental simulations of a comet nucleus, as conducted by the KOSI project, has revealed that spallation of up to mm-sized aggregates occurred even though fined-grained constituents of 4–l0 μm median-size were uniformly mixed in interstitial ices to create the starting material [*Thiel et al.*, 1991; *Gruen et al.*, 1993; *Koelzer*, 1991]. Although the mass of comet Wild 2 could not be determined, the surface gravity of small bodies of this size range can be shown to be of the order of one-thousandth the gravity at the surface of Earth. The attendant small escape velocity permits large particles, decimeter in size, to readily escape the gravitational influence and enter the coma.

[45] Release might be expected to be relatively energetic, since warming will result in the sequential sublimation of different volatiles in the particle aggregates. If these volatiles serve as matrix material that bonds the subcomponents of the aggregate together, their loss will result in particle shedding. This process can occur over a wide range of temperatures, depending on the composition and structure of the aggregate. Highly volatile ice components such as CO, CH_4, and N_2 would sublime at temperatures as low as 35 K. Experimental measurements show that ices of CO_2, NH_3 and CH_3OH will sublime rapidly (>10 μm hr^{-1}) at 100, 115 and 160 K, respectively [*Sandford and Allamandola*, 1993], while ices dominated by H_2O sublime rapidly above 180 to 190 K. Larger molecules, many of them organic, are expected to be present and many of these sublime in the range of 150–300 K [*Bernstein et al.*, 1995]. Thus simple sublimation of multicomponent grains could lead to enhanced disintegration over a wide range of ejection distances as the aggregate and its daughter particles warm and undergo progressively higher-temperature volatile releases.

[46] Warming may also trigger disintegration via a number of processes that involve the conversion of chemical energy to thermal and mechanical energy. Previously isolated constituents become mobilized to react with one another. Equilibria can shift. Furthermore, ices exposed to ionizing radiation accumulate trapped radicals and ions [*d'Hendecourt et al.*, 1982], which can react vigorously once warmed. Even when no reactive species are present, raising the temperature of ices can lead to exothermic phase changes. Amorphous H_2O-rich ices undergo several phase changes as they warm to their sublimation temperature (an amorphous-amorphous transition near 80 K, and an amorphous-cubic and then cubic-hexagonal transition as the ice warms above 125 K [*Jenniskens and Blake*, 1994]). Energy liberated during such phase transitions may further disrupt the particle. Larger aggregates can fission into two or more daughter aggregates if internal pressures from trapped sublimed gases exceed the tensile strength of the aggregate.

[47] Comets are often rich in CH_3OH, up to ~15% relative to H_2O [*Biver et al.*, 2002]. When mixed in the same ice, H_2O and CH_3OH can spontaneously form a Type II H_2O-CH_3OH clathrate when warmed above 125 K [*Blake et al.*, 1991]. For CH_3OH/H_2O ratios greater than 0.15, excess methanol from the enclathration process causes a phase separation to intermingled clathrate and CH_3OH pure ice domains, followed by rapid CH_3OH loss. Such complex transitions would result in expansions, increased porosity, and weakening of the ice grain, with the potential for fragment release.

[48] As reviewed by *Hughes* [1991], the idea that frozen free radicals would provide significant energy upon warming goes back to at least *Donn and Urey* [1956]. The transition of amorphous ice to crystalline ice was examined early on by *Patashnik et al.* [1974] as a mechanism of mechanical energy release for producing outbursts, following their laboratory experiments demonstrating the breakup of ice films formed at very low temperatures. *Sandford and Allamandola* [1988] showed that phase change effects are significant, but that with moderate warming rates the conversion can be sufficiently slow that it is not always explosive in nature.

[49] The range of temperatures extant on the surface of the nucleus of Comet Wild at the time of encounter is not known. Stardust's encounter with Comet Wild 2 occurred at a distance of 1.86 AU from the Sun. At this heliocentric distance the equilibrium temperature of a rapidly rotating black body, T_{eqBB}, would be 203 K. However, the local surface temperature undoubtedly varies from location-to-location on the comet and will depend on local composition and structure, shading, local sublimation activity, rotation period, position of the rotation axis, and so on.

[50] The temperatures of cometary surfaces exposed to sunlight are frequently higher than those predicted for a rapidly rotating black body. For example, the temperatures of the sunlight side of Comet Borrelly were seen by the SWIR imaging spectrograph on Deep Space 1 to vary from <300 K to as high as 345 K [*Soderblom et al.*, 2004] at a heliocentric distance where T_{eqBB} would be about 240 K. This temperature range is close to that expected for a slow-rotating, dark object in thermal equilibrium with incident solar radiation [*Soderblom et al.*, 2004]. Similarly, the Vega spacecraft's IKS infrared spectrometer observed a mean value of about 320 K for the surface of Comet Halley when it was at a heliocentric distance of about 0.8 AU, consistent with the blackbody temperature expected from slow rotation of an essentially inactive dark crust covering a significant part of the surface of the nucleus [*Emerich et al.*, 1987].

[51] Surface temperatures are also seen to exceed T_{eqBB} in ground-based observations of comets in which it is thought

the majority of the infrared flux was due to the cometary nucleus rather than coma dust [*Hanner et al.*, 1985; *Tokunaga and Hanner*, 1985; *Veeder et al.*, 1987]. Again, these higher temperatures are consistent with slow rotation of objects with dark surfaces.

[52] The surface can also be cooled in locations rich in ices that are actively subliming. Such cold spots were not identified on comets Halley or Borrelly, consistent with surfaces dominated by relatively volatile poor, inactive regions. However, local cooling due to ice sublimation may have a larger effect on Wild 2, which appears to have a more active, volatile-rich surface.

[53] Stardust was not equipped to measure the temperature of the surface of the Wild 2 nucleus. However, assuming that Wild 2's rotation rate is not particularly rapid, comparison with measurements of other comets would suggest that typical surface temperatures in sunlit, inactive areas, was probably in the range of 250–300 K. Ice-rich areas undergoing significant sublimation, which appear to be relatively common on Wild 2, could well be colder by 50–100 K.

[54] Independent of nuclear surface temperatures, particles ejected from the nucleus will undergo relatively rapid temperature changes as they move into the coma. Dust in the comae of comets typically is warmer than would be expected for a theoretical blackbody at that heliocentric distance [e.g., *Bregman et al.*, 1987; *Lynch et al.*, 1989; *Hayward et al.*, 2000; *Grün et al.*, 2001; *Harker et al.*, 2002]. Such elevated temperatures are expected since small, micron-sized grains (which typically dominate the thermal spectrum of comets) cannot radiate efficiently at wavelengths much larger than their size [e.g., *Hanner and Campins*, 1986]. Larger grains may also show temperature excesses if they are sufficiently fluffy that their individual components act as independent, small emitters. The extent of the temperature excesses depends on particle size, shape, composition, and albedo [*Krishna Swamy et al.*, 1988, 1989]. As a result, individual dust particles in a cometary coma may equilibrate at very different temperatures. For example, a 1-μm diameter silicate grain at r = 1.32 AU would be expected to reach a temperature of about 320 K, while a similar sized grain of amorphous carbon at this heliocentric distance would achieve temperatures above 600 K due to the strong absorption properties of this material in the UV and visible and its poor infrared emission properties [*Krishna Swamy et al.*, 1988]. Thus grains ejected into the comae of comets would be expected to show a range of increased temperatures, unless they are being actively cooled by the sublimation of component volatiles. Such cooling would only be maintained, of course, until the volatile component was exhausted.

[55] The rate of sublimation of volatiles in coma particles depends on the temperature of the grain and the surface binding energy of the molecules of the relevant volatile material. The residence time, t_r, of a molecule on the surface of an ice in a vacuum is given by

$$t_r = v_o^{-1} \exp(\Delta H_s / kT), \tag{14}$$

where v_o is the lattice vibrational frequency of the molecule within its surface matrix site, ΔH_s is the binding energy of the molecule on the ice surface, k is the Boltzmann constant, and T is the ice temperature in Kelvin. Surface binding energies for a variety of ice systems of astrophysical relevance are given by *Sandford and Allamandola* [1993].

[56] If one assumes that sublimation cools the particle to near the material's sublimation temperature, it is possible to estimate the lifetime of a volatile-rich particle in the coma. For example, pure H_2O ice sublimes rapidly in a vacuum at about 150 K, the lowest temperature expected at the surface of Wild 2 at the time of flyby. At this temperature, the residence time of an H_2O molecule on the surface of the ice is about 30 seconds, i.e., the ice loses a 0.4-nm thick monolayer of H_2O every 30 seconds. At this rate, 1.3×10^{-11} m/s, a 1-μm H_2O grain would completely disappear in about 20 hours. For higher temperatures, or for grains dominated by more volatile molecules (CH_3OH, NH_3, CO_2, CO, N_2), sublimation occurs much more quickly. In addition, sublimation rates could be increased if the particle is warmed above the sublimation temperature by the presence of other light absorbing materials or extra energy from exothermic phase transitions or chemical reactions. There are reasons to believe this is the case since, for the H_2O production rate of Wild 2 at the time of encounter (2×10^{28} molecules/s and 20% active area [*Sekanina*, 2003]), the inferred rate of sublimation is about one order of magnitude higher than this. For reference, the flyby distances of Stardust during the 100 s on either side of closest approach, when the highest density of particles was encountered, were such that the flight time of a particle moving at 10 m/s was 6 to 10 hours.

5. Additional Observational Evidence for Cometary Fragmentation

[57] Many comets exhibit mechanical weakness. The early breakup of comet Shoemaker-Levy 9 under the mild gravity-gradient during its close approach to Jupiter implied very low tensile strength [*Asphaug and Benz*, 1996]. Splitting of comets is a surprisingly common phenomenon [*Sekanina*, 1982, 1997], even when no significant external forces are evident. Shedding of clumps may be occurring even more frequently, at a much smaller scale, below the limits of observability. These events and their aftermath evoke the production of large amounts of smaller debris.

[58] Solar and tidal forces are often insufficient for explaining the splitting or sudden outbursts that many comets have exhibited. Episodic sudden outbursts of coma activity for some comets occurring even at large distances from the sun (e.g., the Halley late outburst at 14 AU), have been interpreted as the result of delayed cumulative thermal effects causing gas pressure buildup [*Sekanina et al.*, 1992]. Early outbursts and/or complete breakup of new comets, such as LINEAR (C/1999 S4) [*Weaver et al.*, 2001; *Farnham et al.*, 2001; *Hadamcik and Levasseur-Regourd*, 2003; *Schulz and Stuewe*, 2002], may be evidence of catastrophic release of stored chemical energy. Macroscopic fragmentation of the nucleus of Hyakutake (C/1996 B2) was indicated by modeling of the behavior of bright condensations that occurred [*Desvoivres et al.*, 2000]. The surface of Wild 2 is highly complex, and the existence of spall craters [*Brownlee et al.*, 2004] is clear demonstration that large

areas of surface, outside the crater cavity itself, can be readily excised under stimulation.

6. Discussion

[59] In addition to explaining the highly variable dust impact rates observed by Stardust while in the Wild 2 coma, aggregate release and fragmentation helps explain a number of other cometary phenomena. These mechanisms may be of fundamental importance on many scales of observation, with implications for a variety of nucleus and coma processes.

[60] Cometary structures in the distant outer comae and termed striae, as seen in comet West (C/1975 V1), were first described by Sekanina as due to the delayed breakup of large fragments far from the nucleus, with a suggested mechanism of centrifugal breakup due to fast rotation rates. The Sekanina-Farrell particle fragmentation concept has been successfully applied elsewhere, including striated dust tails in Hale-Bopp (C/1995 O1) [*Sekanina*, 1976; *Sekanina and Farrell*, 1980, 1982]. The existence of these large objects and their continuing emission of dust is further evidence of the intrinsic weakness and friability of matter in the cometary nucleus.

[61] Extended sources of gaseous parent species include the CN-jets in 1P/Halley [*A'Hearn et al.*, 1986; *Klavetter and A'Hearn*, 1994], presumed to reflect the slow release of volatiles from organic-rich CHON grains, which themselves exhibited strong, nonsystematic fluctuations in flux during the Giotto mission flyby [*Clark et al.*, 1987]. Numerous other extended sources have been detected, including the release of CO, C_2, C_3, and H_2CO molecules [*Greenberg and Li*, 1998]. These may be due to simple slow sublimation from individual particles, but could as easily or in some cases be better explained by progressive exposure of volatiles via fragmentation, as has been suggested by *Gunnarsson et al.* [2002] for CO release from comet 29P/Schwassman Wachmann 1. These authors also point out that as particles fragment, the smaller sizes more easily heat up. Even simple sublimation at great distances from the nucleus reinforces the case for fragmentation since it is a direct indication of composite particles with both volatile and nonvolatile components, which comprise the basic requirements for an aggregate, i.e., a disposable adhesion agent (the volatile component) which cements together more inert grains. Likewise, *Oberc* [2002] has argued that the symmetry of the Halley dust boundary can only be explained by the presence of large particles unaffected by solar radiation pressure, subsequently undergoing fragmentation to produce abundant smaller particles.

[62] Evidence for particle size heterogeneities consistent with clumpy stream components was seen in the missions to comet 1P/Halley. The particle flux and mass distribution in the Halley coma was measured by a range of instruments on three spacecraft in 1986. The DIDSY (Dust Impact Detection System) and PIA (Particle Impact Analyser) experiments on Giotto were used to derive a mass distribution over the range 10^{-18} kg $< m < 10^{-5}$ kg [*McDonnell et al.*, 1987] characterized by four different mass indices (α, the cumulative mass index where the number of particles larger than mass m is $N(m) \propto m^{-\alpha}$). The mass distribution was seen to vary throughout the encounter [*McDonnell et al.*, 1991]. The spatial resolution of the Giotto detectors of 80 km was insufficient to resolve the type of structure seen in 81P/Wild 2 [*Green et al.*, 2004], but there is evidence for structure in the inner coma nonetheless. The deceleration profile of Giotto, derived from the Radio Science Experiment, was used to infer the presence of narrow (<2°) "jets" [*Edenhofer et al.*, 1987], which might also be interpreted a dust clumps of the type described here.

[63] The DUCMA (Dust Counter and Mass Analyser) and SP-1 and SP-2 instruments on VEGA 1 and VEGA 2 sampled the outer coma of 1P/Halley at distances >8000 km. They showed large mass-dependent bursts of activity and changes in the mass distribution for 10^{-18} kg $< m < 10^{-10}$ kg [*Simpson et al.*, 1986, 1987; *Mazets et al.*, 1986, 1987; *Vaisberg et al.*, 1986, 1987]. These were interpreted as narrow jets, with the mass dispersion a result of differential acceleration from gas drag. Again, these might also be consistent with the break up of aggregate particles within broader jet structures, as discussed here. *Simpson et al.* [1987] identified "clusters" and "packets" of particles in DUCMA data and interpreted them as evidence for fragmentation. The nonrandom arrival times of events and the detection of very small particles by all the instruments beyond the nominal coma boundary defined by solar radiation pressure also implied fragmentation from large grains at large cometocentric distances.

[64] Dust particles analyzed by the PIA instrument showed variations in the relative proportions of chemical classes, not only between CHON and Mixed particle types, but also within the CHON subgroups. Time bunching of CHON particles (Figure 2 of *Clark et al.* [1987] at 7 and 2.5 minutes before encounter, respectively) deviated from the more generally smooth pattern, and may be indicative of compositional biases in jets, or clusters of fragments from larger aggregates enriched in the class of particles observed.

[65] The flyby geometry and relative speed of Giotto at Comet 26P/Grigg-Skjellerup in 1992, coupled with the lower activity of the comet, resulted in much lower dust fluxes and prevented a direct investigation of coma structure by the dust impact sensors. However, DIDSY did suggest a mass distribution dominated by larger ($m > 10^{-9}$ kg) grains [*McDonnell et al.*, 1993]. Likewise, the measured Wild 2 particle size distribution also results in the numbers of particles being heavily weighted toward the smaller sizes, but the mass being carried by the higher-sized portion of the distribution [*Green et al.*, 2004]. This mass bias has been somewhat unbounded because of the inevitable poor statistics for large particles because of the short observation times on flyby missions. Heretofore, this open-ended mass assessment has been enigmatic, but it is both consistent with and possibly indicative of significant contributions to overall comet mass loss in the form of larger aggregates of material leaving the surface. These then provide the source for a quasi-continuous distribution of particle sizes, not unlike exponential rock populations on a bombarded planetary surface (again, due to one or more processes of random fragmentation).

[66] The Optical Probe Experiment (OPE) on Giotto observed the integrated scattered light from particles in its narrow field of view as it swept though the coma of Grigg-Skjellerup. It detected several short-lived increases in scat-

tered light, indicating brief enhancements in the dust spatial density in the field of view. *Le Duin et al.* [1996] proposed an explanation in terms of expanding dust shells resulting from impacts directly onto the spacecraft structure. However, *McBride et al.* [1997] showed that the data could not be matched by such a mechanism and proposed an alternative explanation - detection of very narrow "pencil jets" and a possible large (10 to 100 m), eroding or fragmenting object over 1000 km from the nucleus. Again, we suggest that localized clumps of particles due to the break up of larger aggregate grains might be considered as a possible explanation for the short-lived increases in scattered light.

[67] Optical Probe Experiment (OPE) and the Dust Impact Detection System (DIDSY) data for the Halley flyby were reassessed by *Levasseur-Regourd et al.* [1999] following improvements in the analysis and calibration of OPE after Giotto's encounter with Grigg-Skjellerup. *Levasseur-Regourd et al.* [1999] found that the local brightness and dust flux were remarkably consistent, even though the instruments were sampling somewhat different particle size ranges. The data, obtained between around 1,000–100,000 km from the nucleus, showed an overall r^{-2} dependence, although local deviations were seen. For example, within r = 2000 km, the OPE data showed an enhancement, perhaps indicating an excess of small high-albedo icy particles near the nucleus, or conversely, more very large grains (which dominate the scattering cross sectional area as the mass distribution slope would be very shallow) which may then fragment.

[68] Few comets have been within range to be observed with ground-based radar, but radar studies of Hyakutake (C/1996 B2) and others have shown evidence for porous, cm-sized grains near their nuclei and being ejected anisotropically at velocities of 10/s of m/s. Indeed, mass loss by large particle emission of some comets, as assessed by these coma radar echo profiles, may rival their dust and gas mass loss rates [*Harmon et al.*, 1997, 1999]. These high concentrations of cm-sized particles may not persist into the more distant portions of the comae that have been sampled by flyby missions since no particles this large have been detected by in situ measurements. Fragmentation, including severe erosion, is the plausible explanation.

[69] As cometary particles move beyond the drag forces from expanding gases of sublimation, their number density decreases as the inverse-square of the distance but the observational path length for optical scattering increases linearly. Under normal conditions of small total optical depth, the isophote contours should therefore exhibit a net R^{-1} dependence, where R is the distance reference point. Non-R^{-1} behavior for intensity profiles of jets, implying larger particles near the nucleus, has been observed for comet Borrelly and ascribed to dust fragmentation [*Boice et al.*, 2002]. Telescopically observed scattered light from abundant fine-grained coma particulates may derive in significant part from the disintegration products of aggregate clumps of dust grains and ice. However, heterogeneities in coma structure are difficult to detect especially with ground based telescopes and even with imaging systems from flyby spacecraft because these remote observations measure the integrated column density along the line of sight and are dominated by the more numerous smaller particles whose scattering area dominates that of the largest particles, as given in the example above.

[70] Wild 2 may be exceptional because of its possible primitive state, assuming it is truly fresh from the Kuiper belt [*Brownlee et al.*, 2003, 2004]. However, a level of aggregate release and fragmentation may occur in most comets, consistent with radar observations, jet and coma intensity profiles, cometary striae, extended sources of volatiles, episodic outbursts and splitting, bimodal and variable dust size distributions, and extreme pseudocollimation in some jets. Observability of streaming clumps phenomena has been hindered by a lack of resolution on both the temporal and spatial scales for both ground-based observations and in-space missions prior to the Stardust flyby. Closer observations of the innermost coma region near the nucleus during a flyby or a rendezvous mission (Rosetta with Churyumov-Gerasimenko in 2014) could reveal time and spatial variations reflecting the size distribution of the clumps and the release profiles of their constituents. Spatial resolutions at the kilometer scale, or smaller, are needed.

[71] **Acknowledgments.** The authors wish to acknowledge valuable comments on an early manuscript by A.-C. Levasseur-Regourd. We gratefully acknowledge NASA, the Discovery Program, and the office of the Stardust Project for making this mission possible. The continuing efforts of P. Tsou, deputy principle investigator, have significantly facilitated science reporting. S.F.G. acknowledges the financial support of the UK Particle Physics and Astronomy Research Council.

References

A'Hearn, M. F., S. Hoban, P. V. Birch, C. Bowers, R. Martin, and C. A. Klinglesmith (1986), Cynaogen jets in comet Halley, *Nature*, *324*, 649–651.

Asphaug, E., and W. Benz (1996), Size, density and structure of comet Shoemaker-Levy 9 inferred from the physics of tidal breakup, *Icarus*, *121*, 225–248.

Baird, A. K., A. J. Castro, B. C. Clark, P. Toulmin, H. Rose, K. Keil, and J. Gooding (1977), The Viking X-ray Fluorescence Experiment: Sampling strategies and laboratory simulations, *J. Geophys. Res.*, *82*, 4595–4634.

Bernstein, M. P., S. A. Sandford, L. J. Allamandola, S. Chang, and M. A. Scharberg (1995), Organic compounds produced by photolysis of realistic interstellar and cometary ice analogs containing methanol, *Astrophys. J.*, *454*, 327–344.

Biver, N., D. Bockelee-Morvan, J. Crovisier, P. Colom, F. Henry, R. Moreno, G. Paubert, D. Despois, and D. D. Lis (2002), Chemical composition diversity among 24 comets observed at radio wavelengths, *Earth Moon Planets*, *90*, 323–333.

Blake, D., L. Allamandola, S. Sandford, D. Hudgins, and F. Freund (1991), Clathrate hydrate formation in amorphous cometary ice analogs in vacuo, *Science*, *254*, 548–551.

Boice, D. C., D. T. Britt, R. M. Nelson, B. R. Sandel, L. A. Soderblom, N. Thomas, and R. V. Yelle (2002), The near-nucleus environment of 19P/Borrelly during the DS-1 encounter, *Proc. Lunar Planet. Sci. Conf. 33rd*, abstract 1810.

Bregman, J. D., H. Campins, F. C. Witteborn, D. H. Wooden, D. M. Rank, L. J. Allamandola, M. Cohen, and A. G. G. M. Tielens (1987), Airborne and ground-based spectrophotometry of comet P/Halley from 5–13 micrometers, *Astron. Astrophys.*, *187*, 616–620.

Britt, D. T., et al. (2004), The morphology and surface processes of comet 19/P Borrelly, *Icarus*, *167*, 100–112.

Brownlee, D. E., et al. (2003), Stardust: Comet and interstellar dust sample return mission, *J. Geophys. Res.*, *108*(E10), 8111, doi:10.1029/2003JE002087.

Brownlee, D., et al. (2004), Surface of young Jupiter family comet 81P/Wild 2: View from the Stardust spacecraft, *Science*, *304*(5678), 1764–1769.

Clark, B. C., L. W. Mason, and J. Kissel (1987), Systematics of the "CHON" and other light-element particle populations in comet P/Halley, *Astron. Astrophys.*, *187*, 779–784.

Crifo, J.-F., A. V. Rodionov, K. Szego, and M. Fulle (2002), Challenging a paradigm: Do we need active and inactive areas to account for near-nuclear jet activity?, *Earth Moon Planet*, *90*, 227–238.

Desvoivres, E., J. Klinger, A. C. Levasseur-Regourd, and G. H. Jones (2000), Modeling the dynamics of cometary fragments: Application to comet C/1996 B2 Hyakutake, *Icarus*, *144*, 172–181.

d'Hendecourt, L. B., L. J. Allamandola, F. Baas, and J. M. Greenberg (1982), Interstellar grain explosions: Molecule cycling between gas and dust, *Astron. Astrophys.*, *109*, L12–L14.

Donn, B., and H. C. Urey (1956), On the mechanism of cometary outbursts and the chemical composition of comets, *Astrophys. J.*, *123*, 339–342.

Edenhofer, P., M. K. Bird, J. P. Brenkle, H. Buschert, E. R. Kursinski, N. A. Motinger, H. Porsche, C. T. Stelzreid, and H. Volland (1987), Dust distribution of comet P/Halley's inner coma determined from the Giotto Radio-Science Experiment, *Astron. Astrophys.*, *187*, 712–718.

Emerich, C., et al. (1987), Temperature and size of the nucleus of comet P/Halley deduced from IKS infrared Vega 1 measurements, *Astron. Astrophys.*, *187*, 839–842.

Farnham, T. L., D. G. Schleicher, L. M. Woodney, P. V. Birch, C. A. Eberhardy, and L. Levy (2001), Imaging and photometry of comet C/1999 S4 (LINEAR) before perihelion and after breakup, *Science*, *292*, 1348–1353.

Green, S. F., J. A. M. McDonnell, N. McBride, M. T. S. H. Colwell, A. J. Tuzzolino, T. E. Economou, P. Tsou, B. C. Clark, and D. E. Brownlee (2004), Dust mass distribution of comet 81P/Wild 2, *J. Geophys. Res.*, *109*, E12S04, doi:10.1029/2004JE002318.

Greenberg, J. M., and A. Li (1998), From interstellar dust to comets: The extended CO source in comet Halley, *Astron. Astrophys.*, *332*, 374–384.

Gruen, E., et al. (1993), Development of a dust mantle on the surface of an insolated ice-dust mixture: Results fro the KOSI-9 experiment, *J. Geophys. Res.*, *98*, 15,091–15,104.

Grün, E., et al. (2001), Broadband infrared photometry of comet Hale-Bopp with ISOPHOT, *Astron. Astrophys.*, *377*, 1098–1118.

Gunnarsson, M., H. Rickman, M. C. Festou, A. Winnberg, and G. Tancredi (2002), An extended CO source around comet 29P/Schwassmann-Wachmann 1, *Icarus*, *157*, 309–322.

Hadamcik, E., and A.-C. Levasseur-Regourd (2003), Dust coma of comet C/1999 S4 (LINEAR): Imaging polarimetry during nucleus disruption, *Icarus*, *166*, 188–194.

Hanner, M. S., and H. Campins (1986), Thermal emission from the dust coma of comet Bowell and a model for the grains, *Icarus*, *67*, 51–62.

Hanner, M. S., D. K. Aitken, R. Knacke, S. McCorkle, P. F. Roche, and A. T. Tokunaga (1985), Infrared spectrophotometry of Comet IRAS-Araki-Alcock (1983d): A bare nucleus revealed?, *Icarus*, *62*, 97–109.

Harker, D. E., D. H. Wooden, C. E. Woodward, and C. M. Lisse (2002), Grain properties of comet C/1995 O1 (Hale-Bopp), *Astrophys. J.*, *580*, 579–597.

Harmon, J. K., et al. (1997), Radar detection of the nucleus and coma of comet Hyakutake (C/1996 B2), *Science*, *278*, 1921–1923.

Harmon, J. K., D. B. Campbell, S. J. Ostro, and M. C. Nolan (1999), Radar observations of comets, *Planet. Space Sci.*, *47*, 1409–1422.

Hartmann, W. K. (1993), Physical mechanism of comet outbursts: An experimental result, *Icarus*, *104*, 226–233.

Hayward, T. L., M. S. Hanner, and Z. Sekanina (2000), Thermal infrared imaging and spectroscopy of comet Hale-Bopp (C/1995 O1), *Astrophys. J.*, *538*, 428–455.

Hill, J. R., and D. A. Mendis (1980), On the origin of striae in cometary dust tails, *Astrophys. J.*, *242*, 395–401.

Hughes, D. W. (1991), Possible mechanisms for cometary outbursts, in *Comets in the Post-Halley Era*, edited by R. L. Newburn, M. Neugebauer, and J. Rahe, pp. 825–851, Kluwer Acad., Norwell, Mass.

Jenniskens, P., and D. F. Blake (1994), Structural transitions in amorphous water ice and astrophysical implications, *Science*, *265*, 753–756.

Klavetter, J. J., and M. F. A'Hearn (1994), An extended source for CN jets in Comet P/Halley, *Icarus*, *107*, 322–334.

Koelzer, G. (1991), Size distributions of dust particles emitted from mineral-ice mixtures under space conditions, in *Theoretical Modelling of Comet Simulation Experiments*, edited by N. I. Koemle, S. J. Bauer, and T. Spohn, pp. 67–89, Oberreichischen Akad. der Wiss., Vienna.

Krishna Swamy, K. S., S. A. Sandford, L. J. Allamandola, F. C. Witteborn, and J. D. Bregman (1988), A multicomponent model of the infrared emission from Comet Halley, *Icarus*, *75*, 351–370.

Krishna Swamy, K. S., S. A. Sandford, L. J. Allamandola, F. C. Witteborn, and J. D. Bregman (1989), Infrared emission from comets, *Astrophys. J.*, *340*, 537–549.

Le Duin, T., J. F. Crifo, D. Le Queau, and F. A. Crifo (1996), A quantitative interpretation of the in-situ observations of the dust coma of comet P/Grigg-Skjellerup by the OPE photopolarimeter, *Astron. Astrophys.*, *308*, 261–272.

Levasseur-Regourd, A. C. (2004), Cometary dust unveiled, *Science*, *304*, 1762–1763.

Levasseur-Regourd, A. C., N. McBride, E. Hadamcik, and M. Fulle (1999), Similarities between in situ measurements of local dust light scattering and dust flux impact data within the coma of 1P/Halley, *Astron. Astrophys.*, *348*, 636–641.

Lynch, D. K., R. W. Russell, H. Campins, F. C. Witteborn, J. D. Bregman, D. M. Rank, and M. Cohen (1989), 5- to 13-μm airborne observations of comet Wilson 1986I, *Icarus*, *82*, 379–388.

Mazets, E. P., et al. (1986), Comet Halley dust environment from SP-2 detector measurements, *Nature*, *321*, 276–278.

Mazets, E. P., et al. (1987), Dust in comet P/Halley from Vega observations, *Astron. Astrophys.*, *187*, 699–706.

McBride, N., S. F. Green, A.-C. Levasseur-Regourd, B. Goidet-Devel, and J. B. Renard (1997), The inner dust coma of comet 26P/Grigg-Skjellerup: Multiple jets and nucleus fragments?, *Mon. Not. R. Astron. Soc.*, *289*, 535–553.

McDonnell, J. A. M., et al. (1987), The dust distribution within the inner coma of comet P/Halley 1982i: Encounter by Giotto's impact detectors, *Astron. Astrophys.*, *187*, 719–741.

McDonnell, J. A. M., P. L. Lamy, and G. S. Pankiewicz (1991), Physical properties of cometary dust, in *Comets in the Post-Halley Era*, vol. 2, edited by R. L. Newburn, M. Neugebauer, and J. Rahe, pp. 1043–1073, Kluwer Acad., Norwell, Mass.

McDonnell, J. A. M., et al. (1993), Dust particle impacts during the Giotto encounter with comet Grigg-Skjellerup, *Nature*, *362*, 732–734.

Oberc, P. (2002), On the dust boundary at Halley and volatility of cometary organics, in *Proceedings of Asteroids, Comets, Meteors - ACM 2002*, edited by B. Warmbein, *Eur. Space Agency Spec. Publ.*, *ESA-SP 500*, 579–582.

Patashnik, H., G. Rupprecht, and D. W. Schuerman (1974), Energy source for cometary outburst, *Nature*, *250*, 313–314.

Sandford, S. A., and L. J. Allamandola (1988), The condensation and vaporization behavior of H_2O:CO ices and implications for interstellar grains and cometary behavior, *Icarus*, *76*, 201–224.

Sandford, S. A., and L. J. Allamandola (1993), Condensation and vaporization studies of CH_3OH and NH_3 ices: Major implications for astrochemistry, *Astrophys. J.*, *417*, 815–825.

Schulz, R., and J. A. Stuewe (2002), The dust coma of comet C/1994 S4 (LINEAR), *Earth Moon Planets*, *90*, 195–203.

Sekanina, Z. (1976), Progress in our understanding of cometary dust tails, in *The Study of Comets*, edited by B. Donn et al., *NASA Spec. Publ.*, *NASA-SP 393*, 893–939.

Sekanina, Z. (1982), The problem of split comets in review, in *Comets*, edited by L. L. Wilkening, pp. 251–287, Univ. of Ariz., Tucson.

Sekanina, Z. (1997), The problem of split comets revisited, *Astron. Astrophys.*, *318*, L5–L8.

Sekanina, Z. (2003), A model for comet 81P/Wild 2, *J. Geophys. Res.*, *108*(E10), 8112, doi:10.1029/2003JE002093.

Sekanina, Z., and J. A. Farrell (1980), Evidence for fragmentation of strongly nonspherical dust particles in the tail of Comet West 1976 VI, in *Solid Particles in the Solar System*, edited by I. Halliday, pp. 267–270, Springer, New York.

Sekanina, Z., and J. A. Farrell (1982), Two dust populations of particle fragments in the striated tail of Comet MRKOS 1957 V, *Astron J.*, *87*, 1836–1853.

Sekanina, Z., S. M. Larson, O. Hainaut, A. Smette, and R. M. West (1992), Major outburst of periodic Comet Halley at a heliocentric distance of 14 AU, *Astron. Astrophys.*, *263*, 367–386.

Sekanina, Z., D. E. Brownlee, T. E. Economou, A. J. Tuzzolino, and S. F. Green (2004), Modeling the nucleus and jets of comets 81P/Wild 2 based on the Stardust encounter data, *Science*, *304*, 1769–1774.

Simpson, J. A., et al. (1986), Dust counter and mass analyser (DUCMA) measurements of comet Halley's coma from Vega spacecraft, *Nature*, *321*, 278–280.

Simpson, J. A., D. Rabinowitz, A. J. Tuzzolino, L. V. Ksanfomality, and R. Z. Sagdeev (1987), The dust coma of comet P/Halley: Measurements on the Vega-1 and Vega-2 spacecraft, *Astron. Astrophys.*, *187*, 742–752.

Soderblom, L. A., D. T. Britt, R. H. Brown, B. J. Buratti, R. L. Kirk, T. C. Owen, and R. V. Yelle (2004), Short-wavelength infrared (1.3–2.6 μm) observations of the nucleus of comet 19P/Borrelly, *Icarus*, *167*, 100–112.

Thiel, K., G. Koelzer, and H. Kohl (1991), Dust emission of mineral/ice mixtures: Residue structure and dynamical parameters, *Geophys. Res. Lett.*, *18*, 281–284.

Tokunaga, A. T., and M. S. Hanner (1985), Does comet P/Arend-Rigaux have a large dark nucleus?, *Astrophys. J.*, *296*, L13–L16.

Tsou, P., D. E. Brownlee, S. A. Sandford, F. Hörz, and M. E. Zolensky (2003), Wild 2 and interstellar sample collection and Earth return, *J. Geophys. Res.*, *108*(E10), 8113, doi:10.1029/2003JE002109.

Tsou, P., et al. (2004), Stardust encounters comet 81P/Wild 2, *J. Geophys. Res.*, *109*, E12S01, doi:10.1029/2004JE002317.

Tuzzolino, A. J., T. E. Economou, B. C. Clark, P. Tsou, D. E. Brownlee, S. F. Green, J. A. M. McDonnell, N. McBride, and M. T. S. H. Colwell (2004), Dust measurements in the coma of comet Wild 2 by the Dust Flux Monitor Instrument, *Science*, *304*(5678), 1776–1780.

Vaisberg, O. L., et al. (1986), Dust coma structure of comet Halley from SP-1 detector measurements, *Nature*, *321*, 274–276.

Vaisberg, O. L., V. Smirnov, A. Omelchenko, L. Gorn, and M. Iovlev (1987), Spatial and mass distributions of low-mass dust particles ($m < 10^{-10}$ g) in comet P/Halley's coma, *Astron. Astrophys.*, *187*, 753–760.

Veeder, G. J., M. S. Hanner, and D. J. Tholen (1987), The nucleus of comet P/Arend-Rigaux, *Astron. J.*, *94*, 169–173.

Weaver, H. A., et al. (2001), HST and VLT Investigations of the Fragments of Comet C/1999 S4 (LINEAR), *Science*, *292*, 1329–1333.

Whipple, F. L. (1951), A comet model II. Physical relations for comets and meteors, *Astrophys. J.*, *113*, 464–474.

Yelle, R. V., L. A. Soderblom, and J. R. Jokipii (2004), Formation of jets in comet 19P/Borrelly by subsurface geysers, *Icarus*, *167*, 30–36.

D. E. Brownlee, Astronomy Department, University of Washington, Box 351580, Seattle, WA 98195, USA.

B. C. Clark, Lockheed Martin, P.O. Box 179, MS-S8000, Denver, CO 80201, USA. (benton.c.clark@lmco.com)

T. E. Economou, Laboratory for Astrophysics and Space Research, Enrico Fermi Institute, University of Chicago, 933 East 56th Street, Chicago, IL 60637, USA.

S. F. Green and N. McBride, Planetary and Space Sciences Research Institute, Open University, Walton Hall, Milton Keynes MK7 6AA, UK.

S. A. Sandford, NASA Ames Research Center, MS 245-6, Moffett Field, CA 94035, USA.

M. E. Zolensky, NASA Johnson Space Center, Code ST, Houston, TX 77058, USA.